



**QUEEN'S
UNIVERSITY
BELFAST**

Factors influencing the compressive strengths of fly ash based geopolymers

Soutsos, M., Boyle, A. P., Vinai, R., Hadjierakleous, A., & Barnett, S. J. (2016). Factors influencing the compressive strengths of fly ash based geopolymers. *Construction and Building Materials*, 110, 355-368. <https://doi.org/10.1016/j.conbuildmat.2015.11.045>

Published in:
Construction and Building Materials

Document Version:
Peer reviewed version

Queen's University Belfast - Research Portal:
[Link to publication record in Queen's University Belfast Research Portal](#)

Publisher rights

© 2016 Elsevier Ltd. This manuscript version is made available under the CC-BY-NC-ND 4.0 license <http://creativecommons.org/licenses/by-nc-nd/4.0/> which permits distribution and reproduction for non-commercial purposes, provided the author and source are cited.

General rights

Copyright for the publications made accessible via the Queen's University Belfast Research Portal is retained by the author(s) and / or other copyright owners and it is a condition of accessing these publications that users recognise and abide by the legal requirements associated with these rights.

Take down policy

The Research Portal is Queen's institutional repository that provides access to Queen's research output. Every effort has been made to ensure that content in the Research Portal does not infringe any person's rights, or applicable UK laws. If you discover content in the Research Portal that you believe breaches copyright or violates any law, please contact openaccess@qub.ac.uk.

Open Access

This research has been made openly available by Queen's academics and its Open Research team. We would love to hear how access to this research benefits you. – Share your feedback with us: <http://go.qub.ac.uk/oa-feedback>

1 Factors influencing the compressive strength of fly ash 2 based geopolymers

3 Marios Soutsos¹, Alan P. Boyle², Raffaele Vinai¹, Anastasis Hadjierakleous², and Stephanie J. Barnett³

4 ¹ School of Planning, Architecture and Civil Engineering, Queen's University Belfast, BT9 5AG, UK

5 ² School of Environmental Sciences, University of Liverpool, L69 3GP, UK

6 ³ School of Civil Engineering and Surveying, University of Portsmouth, PO1 2UP, UK

7 **Abstract**

8 Several factors affecting the reactivity of fly ash (FA) as a precursor for geopolymer concrete have been
9 investigated. These include physical and chemical properties of various FA sources, inclusion of ground
10 granulated blast furnace slag (ggbs), chemical activator dosages and curing temperature. Alkali-activated FA
11 was found to require elevated curing temperatures and high alkali concentrations. A mixture of sodium
12 hydroxide and sodium silicate was used and this was shown to result in high strengths, as high as 70 MPa at 28
13 days. The presence of silicates in solution was found to be an important parameter affecting strength. Detailed
14 physical and chemical characterisation was carried out on thirteen FA sources from the UK. The most
15 important factor affecting the reactivity was found to be the particle size of FA. The loss on ignition (LOI) and
16 the amorphous content are also important parameters that need to be considered for the selection of FA for
17 use in geopolymer concrete. The partial replacement of FA with ggbs was found to be beneficial in not only
18 avoiding the need for elevated curing temperatures but also in improving compressive strengths.
19 Microstructural characterisation with scanning electron microscope (SEM) coupled with energy dispersive X-
20 ray spectroscopy (EDS) was performed on FA/ggbs pastes. The reaction product of FA and ggbs in these binary
21 systems was calcium aluminium silicate hydrate gel (C-A-S-H) with inclusion of Na in the structure.

22 **Keywords:** geopolymer, alkali activated material, fly ash, slag, structural characterisation, mechanical
23 properties, alkali dosages optimisation

24 **1 Introduction**

25 The term "geopolymer" was introduced by Davidovits in the 1970s referring to alkali-activated metakaolin [1].
26 It has since been used for a range of synthetic low-calcium aluminosilicate polymeric materials, as a sub-range
27 of a more general definition which is alkali-activated binders (AAB). Although the initial studies were focused

28 on geological materials such as metakaolin activated with siliceous solutions [2-6], the potential of using other
29 synthetic reactive aluminosilicate materials activated with a range of concentrated alkaline solutions became
30 apparent [1,7-8].

31 AABs have been studied for the last 40 years [9] and have applications in ceramics, hazardous waste
32 containment, fire-resistant construction materials and refractories [10, 11]. One of the most interesting
33 applications is their use as a cement-free binder that can replace Portland cement-based pastes in
34 construction materials such as concrete and mortar products [12].

35 Geopolymers can provide a desirable alternative to Portland cement (PC) binders, not only for the
36 environmental benefits arising from the avoidance of CO₂ emissions associated with PC production, but also in
37 terms of their performance and durability, where such properties are not only equivalent, but often better
38 than those achieved with PC. The nature of the reactions occurring in geopolymerisation can be summarized in
39 three basic steps [13]:

- 40 1. *Dissolution of the aluminosilicate solids:* aluminosilicates in the pozzolanic solid are dissolved by
41 alkaline hydrolysis in the high pH solution of the concentrated alkaline activator. This forms a solution
42 of silicate, aluminate and aluminosilicate species.
- 43 2. *Gel Formation:* species released by dissolution are held in the aqueous phase, which may also contain
44 silicate present from the activating solution. This supersaturated aluminosilicate solution forms a gel
45 as oligomers form long chains and networks. This stage releases complexing water, which resides in
46 pores.
- 47 3. *Polycondensation:* the gel species continue to rearrange and reorganize, forming an increasingly
48 larger network. This results in the three-dimensional aluminosilicate network of the geopolymer
49 binder.

50 These processes often occur contemporaneously throughout the mixture, rather than in a linear time series.
51 The dense inorganic polymer that forms the geopolymer binder thus provides physicochemical features that
52 may be superior to Portland cement systems, i.e.:

- 53 • The interconnected framework gives geopolymers high compressive strengths [13, 14].

- 54 • Due to the microstructure of the reaction products, geopolymer and AAB can show good to very good
55 resistance to chemical degradation (sulphate attack, acid attack, seawater attack) [9].
- 56 • The geopolymer matrix shows high thermal and fire resistance up to 1000-1200 °C [14].
- 57 • Geopolymers may exhibit rapid setting without long term deterioration of strength [13].

58 Of particular interest is the selection of precursor aluminosilicate materials that arise from waste-streams or as
59 by-product pozzolans, which are readily available from existing industries [15]. These include fly ash (FA) and
60 ground granulated blast furnace slag (ggbfs). Although ggbfs has a relatively high demand from an existing
61 market-base, and an associated relatively high value, perhaps equivalent to that of Portland cement, waste-
62 stream pozzolans such as FA are not fully recycled into value added products, and excesses are stockpiled or
63 landfilled.

64 Reaction mechanisms responsible for the creation of an amorphous gel from fly ash are complex and still not
65 fully understood [9]. A wide variability in chemical dosages can be found in the scientific literature related to
66 the activation of FA systems [16], indicating that optimum proportions of alkali species (hydroxides and
67 silicates) in the activating solution, as well as quantity of alkali per binder mass, still need to be investigated to
68 improve our understanding of the reaction mechanisms. Curing parameters such as curing temperature and
69 stand time, i.e. the time elapsed before the start of high temperature curing, play an important role in the full
70 development of the reaction products. Information available in technical literature is relatively limited, and
71 thus a systematic investigation is still needed for determining optimum curing conditions.

72 Fly ashes are not a “standard product” as their physical and chemical properties vary considerably not only
73 from source to source but also over time from the same power station [9]. The Department of Energy and
74 Climate Change in its digest of UK energy statistics [17] quoted 14 power stations operational at the end of
75 May 2014 that were using coal or coal mixed (gas/oil) fuel, representing 26% of total electricity generated.
76 Heath et al. [18] reported that FA production in UK is estimated at about $6 \cdot 10^6$ t per annum, half of which is
77 sent to landfill, whereas about $114 \cdot 10^6$ t of FA is available in stockpiles. The potential availability for FA-based
78 geopolymer concrete production is therefore significant in the UK, although the suitability of such available
79 ashes has never been investigated in a comprehensive manner.

80 FA-based geopolymers need an external energy source in the form of thermal curing for the reaction to take
81 place. This can be a drawback for the upscaling of the process to the industrial level. On the other hand, Ca-
82 rich slags such as ggbs react at room temperature since their reaction, i.e. the hydration of Ca species and the
83 creation of a calcium-aluminium-silicate-hydrate (C-A-S-H) gel, is different from low-calcium precursors.
84 Moreover, the reaction develops at a very rapid pace, often resulting in a very short initial setting time. The
85 blend of FA/ggbs for achieving a system reacting at room temperature without rapid setting would suit most
86 concrete applications. Relatively few publications are available in the literature [19-23] and thus further
87 investigations are needed to provide a better insight into the properties and performance of such binary
88 systems.

89 The work described here aimed to study (a) the effect of curing procedure and activator dosages on the
90 strength development of FA-based mortar, (b) the influence of physical and chemical properties of 13 FA
91 sources obtained from 8 UK power stations, (c) the effect of partial substitution with ggbs on the compressive
92 strength development and microstructure of the reacted mortar.

93 **2 Materials and Methods**

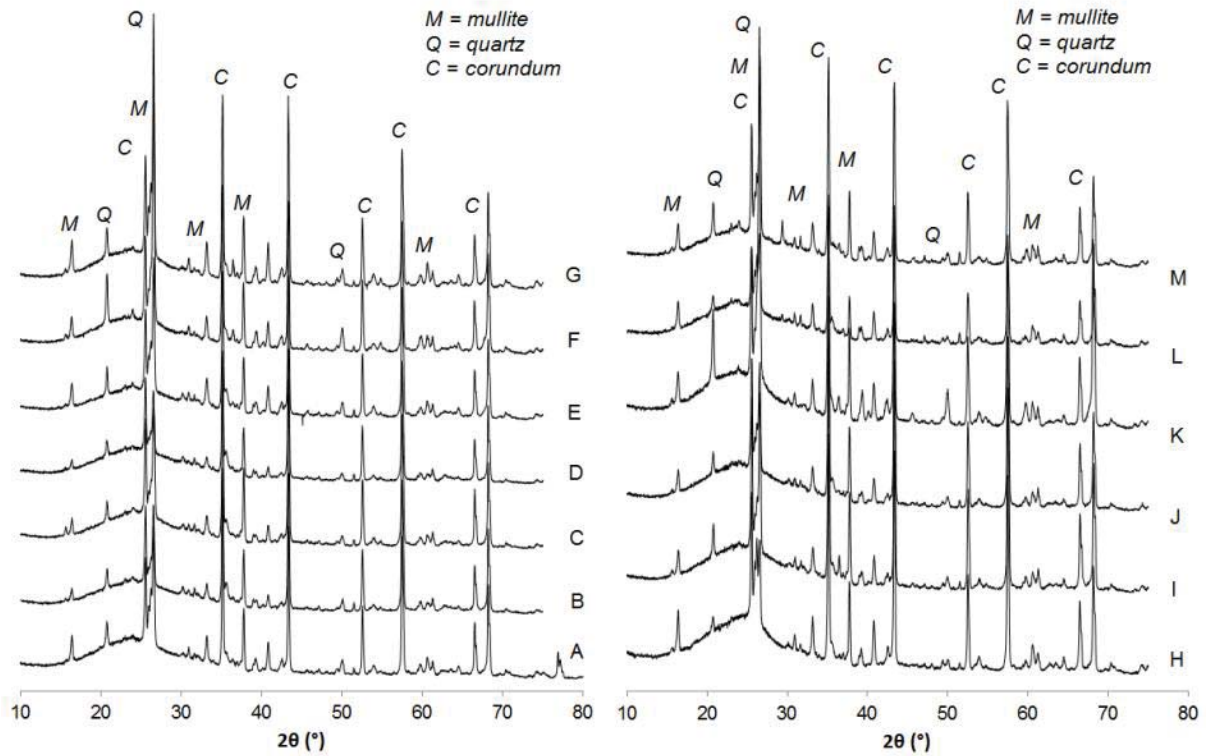
94 The chemical composition of 13 FA sources from the UK were assessed by X-ray fluorescence (XRF) at the
95 University of Leicester and these are shown in Table 1. Loss on Ignition (LOI) was determined on powders
96 previously dried overnight at 105°C. Samples were ignited for 90 minutes @ 950°C in air ventilated electric
97 muffle furnace and the mass loss was then calculated. Mineralogical characterisation was carried out by X-ray
98 diffraction (XRD) using a PANalytical X'Pert PRO X-ray diffractometer, equipped with programmable anti
99 scatter slits, rotating sample stage and the X'Celerator Real Time Multiple Strip X'lerator Detector. The incident
100 X-rays were from a Copper K α X-ray source, running at 40 kV and 40 mA and obtained spectra are shown in
101 Figure 1. Quartz (SiO₂) and mullite (3Al₂O₃·2SiO₂) were the main crystalline components identified. The
102 amorphous content (visible as the broad hump in the background of the XRD pattern centred at 20 – 30° 2 θ)
103 was quantified by adding an internal standard (corundum) and performing a Rietveld method-based analysis
104 (results are shown in Table 2). Laser diffraction grain size distribution was used to assess the particle size
105 distribution of all the investigated sources of FA. Results are shown in Figure 2, where the 13 FA samples are
106 divided in three classes according to their D₅₀ value (shown in Table 2): low (D₅₀ < 25 μ m), medium (26 < D₅₀ <

107 30.5 μ m), and high ($D_{50} > 30.5\mu$ m). FA A was the only one used to study the effect of curing procedure and
 108 activator dosages.

109 **Table 1.** Elemental composition (from XRF) of the 13 FA sources investigated and of the ggbs utilised. Results
 110 quoted as component oxide (and LOI) weight percent.

Oxide	FA sources													ggbs
	A	B	C	D	E	F	G	H	I	J	K	L	M	
SiO ₂	51.52	48.90	44.58	49.28	48.48	56.40	51.32	43.38	51.33	51.05	51.23	49.90	51.76	35.82
TiO ₂	0.97	0.95	0.91	0.95	1.08	0.92	1.03	0.84	0.97	1.02	0.80	1.02	0.89	0.00
Al ₂ O ₃	23.58	23.51	21.94	23.43	24.86	22.14	24.85	23.63	24.12	25.06	18.37	27.12	24.51	13.00
Fe ₂ O ₃	7.11	12.36	10.59	10.61	9.49	6.63	7.24	6.56	8.51	8.60	4.55	7.38	8.58	0.53
Mn ₃ O ₄	0.07	0.15	0.13	0.10	0.12	0.07	0.09	0.13	0.11	0.09	0.06	0.08	0.15	0.51
MgO	1.75	1.97	1.93	1.73	2.22	1.59	1.56	1.36	1.92	1.79	1.36	1.45	1.92	8.00
CaO	3.86	3.41	3.61	2.68	4.53	2.97	2.88	2.83	2.75	2.37	2.55	2.25	3.78	40.62
Na ₂ O	0.74	0.93	0.83	1.55	0.98	0.97	0.57	0.79	0.80	0.98	0.45	0.67	0.49	0.00
K ₂ O	2.42	3.26	2.61	3.57	2.60	1.91	1.63	1.39	3.61	3.47	1.60	3.23	2.87	0.00
P ₂ O ₅	0.37	0.41	0.38	0.32	0.45	0.58	0.75	0.72	0.25	0.33	0.61	0.33	0.25	0.00
SO ₃	0.84	0.49	0.59	0.47	0.63	0.47	0.41	0.28	0.49	0.32	0.39	0.18	0.32	0.05
V ₂ O ₅	0.09	0.06	0.06	0.07	0.07	0.05	0.06	0.03	0.06	0.07	0.03	0.06	0.05	0.00
Cr ₂ O ₃	0.02	0.02	0.02	0.02	0.03	0.02	0.03	0.01	0.02	0.03	0.01	0.02	0.02	0.00
SrO	0.10	0.08	0.08	0.07	0.15	0.12	0.13	0.15	0.06	0.07	0.15	0.07	0.05	0.00
ZrO ₂	0.00	0.07	0.06	0.07	0.07	0.07	0.07	0.11	0.06	0.07	0.07	0.06	0.06	0.00
BaO	0.14	0.14	0.14	0.14	0.20	0.20	0.18	0.26	0.15	0.16	0.22	0.21	0.18	0.00
NiO	0.02	0.02	0.02	0.02	0.02	0.02	0.02	0.01	0.01	0.02	0.01	0.02	0.01	0.00
CuO	0.02	0.02	0.02	0.02	0.02	0.01	0.02	0.00	0.01	0.02	0.00	0.02	0.01	0.00
ZnO	0.04	0.04	0.03	0.04	0.06	0.04	0.06	0.02	0.04	0.04	0.01	0.06	0.01	0.00
PbO	0.03	0.04	0.03	0.05	0.04	0.05	0.06	0.02	0.04	0.04	0.02	0.05	0.02	0.00
LOI	4.92	3.60	11.17	5.01	4.07	4.61	6.99	17.40	4.62	4.53	17.28	5.20	4.28	0.66
Total	98.61	100.43	99.73	100.20	100.17	99.84	99.95	99.92	99.93	100.13	99.77	99.38	100.21	99.19

111



112
 113 **Figure 1.** XRD spectra for the 13 investigated FA sources. Labels A-M equate to labels A-M in Table 1.

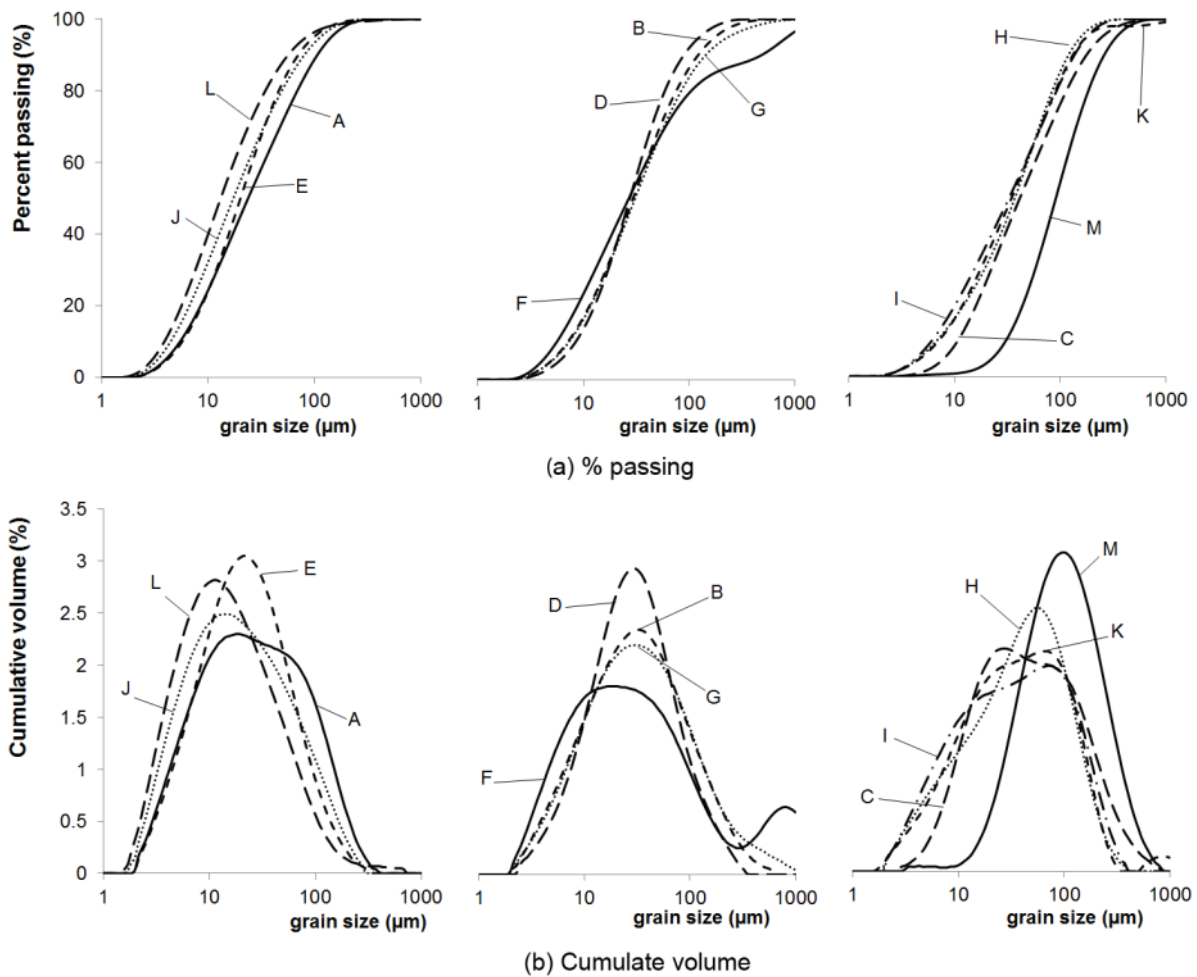
114
 115
 116 **Table 2.** Physical properties of the 13 FA sources investigated.

	A	B	C	D	E	F	G	H	I	J	K	L	M
D_{50} (μm)	23.8	29.2	41.6	27.3	20.2	26.5	30.5	37.3	32.9	17.3	34.7	13.2	91.2
Am.% ¹	82	89	86	90	79	76	75	83	86	87	75	79	81
% 45 μm ²	66.9	63.2	51.0	69.0	77.6	62.4	61.0	54.9	57.3	76.4	56.4	84.8	18.9

117 ¹Amorphous content from XRD Rietveld method quantification

118 ² Volume percentages passing at 45 μm

119
 120
 121
 122



123
124
125
126

Figure 2. Grain size distribution curves for the 13 investigated FA sources. Labels A-M equate to those in Fig. 1 and Table 1.

127 Ground granulated blast furnace slag was supplied by Hanson Ltd. The chemical composition was obtained by
128 XRF analysis and detected oxides are shown in Table 1.

129 Commercially available alkalis were used. Laboratory grade sodium hydroxide (NaOH) in solid form was
130 dissolved in water at the required dosage, whereas sodium silicate was supplied as a solution with the
131 following composition: 12.8% Na₂O, 25.5% SiO₂ and 61.7% H₂O. The alkali dosage (M+) was defined as the
132 percentage mass ratio of total sodium oxide (Na₂O) in the activating solution to the binder. The alkali modulus
133 (AM) was defined as the mass ratio of sodium oxide to silica in the activating solution. M+ was from 7.5% to
134 15%, whereas AM was from 0.5 to ∞ for the first series of experiments. The 0.5 corresponds to an all sodium
135 silicate solution and ∞ corresponds to an all sodium hydroxide solution. A range of dosages were used to find
136 which values gave the maximum strength. These values were then used in subsequent experiments

137 investigating the influence of physical and chemical properties of different FA sources. For the assessment of
138 the effect of partial substitution with ggbs on the compressive strength development and microstructure of
139 the reacted mortar, AM was fixed at 1.25, whilst the M+ was varied from 3% to 10%.

140 The water/solids ratio was defined as the ratio between total mass of water (i.e. added water mass + water
141 mass in the alkali solutions) and the total solid mass (i.e. mass of binder + mass of alkali solids). This ratio was
142 kept constant at 0.37, except when the mixture was found to be of very low consistency after mixing. In such
143 cases, additional water was added until a workable mixture was obtained. This was generally only necessary
144 for 100% ggbs binder.

145 Well-graded, rounded quartz sand sized 0/5 mm was used for preparation of mortars. The adopted
146 sand/binder mass ratio was equal to 2.75. A 5 l planetary mixer was used. Binder and sand were placed in the
147 mixer bowl and mixed for one minute. The alkali solution was then added and the material was mixed for a
148 further 9 minutes. A flow table test was then performed according to BS EN 12350-5 [24]. Mixing was
149 continued for a further 5 minutes, giving a total mixing time of 15 minutes. The mortar was then transferred to
150 50 mm cube moulds and compacted on a vibrating table for 60 seconds. Moulds were then sealed by wrapping
151 in polyethylene film.

152 In the first series of mixes, four sets of curing conditions were used: (a) 1 hour at 20°C followed by curing at
153 50°C; (b) 24 hours at 20°C followed by curing at 50°C; (c) 1 hour at 20°C followed by curing at 70°C; (d) 24
154 hours at 20°C followed by curing at 70°C. One cube from each curing regime was tested in compression after 1,
155 3 and 7 days curing, with two cubes from each curing regime tested at 28 days. Stand time and oven curing
156 time were included for the computation of the total curing time. Some of the mixes were replicated to confirm
157 the reliability of the results. A 300 kN capacity compression testing machine was used for all testing with a
158 loading rate of 0.8 kN/s.

159 In the second series of mixes, two sets of curing conditions were used: (a) 1 hour at 20°C followed by curing at
160 50°C and (b) 1 hour at 20°C followed by curing at 70°C. Same procedure as in the first series of mixes was used
161 for determining the compressive strength.

162 In the third series of mixes, two sets of curing conditions were used: (a) 1 hour at 20°C followed by curing at
163 70°C and (b) curing at 20°C (ambient/room temperature). Two replica cubes from each curing regime were
164 tested in compression at 1, 7 and 28 days.

165 X-ray diffraction on raw materials and reacted pastes was carried out with Panalytical X'Pert Pro MPD
166 Diffractometer with X'Celerator detector scanned the range of 4-70°2θ, using Cu K-α radiation. Zincite was
167 used as internal standard. HighScore Plus software was used to obtain semi-quantitative mineral weight
168 percentages.

169 Images for microstructural analysis were acquired with either a Philips XL30 Scanning Electron Microscope
170 equipped with an Oxford Instruments INCA energy dispersive X-ray spectroscopy (EDS) system or a Hitachi
171 TM300 SEM equipped with a Bruker Quantax 70 EDS systems. The EDS systems allow the collection of
172 chemical information for spots and areas in the samples. The samples comprised broken pieces (~5.0 x 5.0 x
173 2.5 mm) of hardened paste mounted onto aluminium stubs using epoxy adhesive, orienting the fractured
174 surface in a convenient position towards the SEM beam also bearing in mind the location of the EDS detector.
175 Samples were coated with a thin gold-palladium layer to provide a conductive pathway to prevent surface
176 electrical charging.

177 **3 Results and discussion**

178 **3.1 Effect of curing procedure and activator dosages on strength development**

179 Twenty-four combinations of M+ and AM were investigated for each of the four curing regimes, for a total
180 number of 96 different series of mixes. The effects of stand time (i.e. the time elapsed between the mixing and
181 the start of the curing in oven, during which the process of dissolution and gelation of aluminosilicates species
182 takes place), curing temperature, and activator dosage were investigated by determining the compressive
183 strength development. Obtained compressive strengths are shown in Table 3.

184

185

186 **Table 3.** Compressive strengths for mortars produced with varying stand time, curing temperature, and
 187 chemical dosages. Results are expressed in MPa.

AM	Curing time (days)	1 h stand time				50° curing				24 h stand time				50° curing				1 h stand time				70° curing				24 h stand time				70° curing									
				M+				M+				M+				M+				M+				M+				M+				M+				M+			
		7.5	10	12.5	15	7.5	10	12.5	15	7.5	10	12.5	15	7.5	10	12.5	15	7.5	10	12.5	15	7.5	10	12.5	15	7.5	10	12.5	15	7.5	10	12.5	15	7.5	10	12.5	15		
0.5	1	5.4												9.7 10.1												13.6 14.7													
	3	20.2								14.0 11.3				13.0 14.8								13.7 16.4																	
	7	17.3	28.3			17.9	24.2			11.7	13.9			13.7	16.4			12.7	15.8			14.5	18.2																
	28	23.6				17.5 18.2				13.0 14.4				12.7 15.8																									
1	1	8.5	7.5	7.7	3.9									25.4 32.3 36.6 36.4																									
	3	15.7	17.4	27.5	26.9	14.6	15.8	22.4	19.4	40.9	47.4	49.5	53.5	38.1	38.3	45.0	56.1																						
	7	19.1	15.7	24.4	33.8	20.7	13.6	24.5	39.0	43.6	44.8	51.9	52.0	42.5	44.1	47.1	54.3																						
	28	23.9	12.4	24.0	28.2	24.0	13.3	23.4	28.7	41.5	46.0	51.6	50.8	44.3	41.0	49.9	49.4																						
1.25	1	6.6	7.7	5.9	2.6									23.0 32.4 39.3 40.6																									
	3	17.0	16.3	25.7	21.4	13.4	15.1	23.1	14.1	37.8	49.3	63.9	63.4	37.6	42.1	57.8	44.6																						
	7	21.8	18.2	24.4	24.6	22.1	15.8	24.5	25.1	37.1	48.6	63.0	53.3	43.6	50.4	69.5	46.9																						
	28	23.5	19.6	23.4	22.9	23.2	18.6	23.1	24.4	38.3	49.4	59.5	55.5	42.3	46.7	64.4	48.1																						
1.5	1	4.2	4.9	4.8	2.2									18.3 26.8 38.9 39.1																									
	3	15.7	17.3	21.7	17.8	13.7	14.5	17.3	12.4	30.1	37.6	64.5	63.0	25.1	43.5	51.9	41.4																						
	7	20.5	20.5	29.5	23.1	22.7	17.5	24.0	23.0	29.5	39.9	58.2	57.1	26.9	44.3	60.8	45.1																						
	28	23.9	22.7	21.9	23.5	24.3	19.6	24.8	25.5	27.7	44.6	61.3	57.2	37.4	46.3	61.6	49.9																						
2	1	2.3	3.1	3.5	1.7									11.4 21.6 34.7 29.9																									
	3	8.9	15.4	23.4	19.2	8.9	12.0	13.9	10.3	17.3	27.3	57.0	28.3	18.9	32.3	59.8	44.3																						
	7	13.7	24.5	24.1	22.9	14.1	24.1	27.2	37.5	15.7	32.6	57.5	24.2	20.0	35.6	55.9	55.2																						
	28	15.4	24.8	23.3	24.5	16.2	27.6	23.6	36.2	17.9	35.8	57.9	24.3	19.2	37.1	58.3	53.6																						
8	1	1.0 0.0												6.4 14.3 16.5 9.9																									
	3	7.8	12.6	7.5	3.1	4.5	3.9	19.8	1.5	10.3	23.1	24.8	22.5	11.9	22.8	37.5	35.5																						
	7	9.8	14.5	19.6	21.4	9.1	18.1	21.8	25.7	11.6	22.6	28.1	25.7	12.9	23.1	27.8	26.4																						
	28	10.7	17.0	19.4	18.1	10.7	16.9	19.3	24.9	13.4	24.8	31.9	26.0	14.2	27.0	33.2	35.8																						

188

189 *3.1.1 Effect of stand time at 20 °C*

190 In order to assess the effect of the time for dissolution and gelation at room temperature on ultimate strength,
 191 half the samples in each mix were left to stand for 1 hour prior to oven curing and half for 24 hours. Figure 3
 192 shows the results for the 28-day tests for the all mixes cured at 70 °C. It was observed that compressive

193 strength increased from day 1 to day 7, and then the strength gain was small, with 7-day and 28-day strengths
194 being often similar. For this reason, it was considered appropriate to compare 28-day strengths of 1h and 24h
195 stand time samples, as the difference in curing time in the oven (27 vs. 28 days) can be considered negligible.
196 In general, the difference in strength at 28 days between those initially left to stand for 1 hour and those left
197 for 24 hours is small, with the compressive strengths for most mixes being within 6 MPa of each other. The
198 highest alkali dosage (M+ 15%) gave mixed results, with higher strength for 1 h stand time for high dosages of
199 silicate solution (AM = 1.25 and 1.5) and the opposite for low dosages (AM = 2 and ∞). This might be explained
200 by the fact that reactive silicates trigger the nucleation of gel and therefore, when a significant amount is
201 present (lower AM), the gel formation can start immediately and it is enhanced by the high temperature. On
202 the contrary, when the addition of silicates is low (higher AM), the system needs first to achieve the
203 dissolution of Si and Al from the precursor material by the alkali solution at room temperature, whereas the
204 thermal treatment starts the solidification of the gel without allowing enough time for the liquid to complete
205 the dissolution process. Although the difference between no stand time and some stand time can make a
206 difference on strengths by increasing the time for early dissolution and gelation, there appears to be no
207 benefit in leaving mixes for longer than 1 hour between mixing and oven curing. This may be of importance
208 when considering transferring the technology to industry.

209

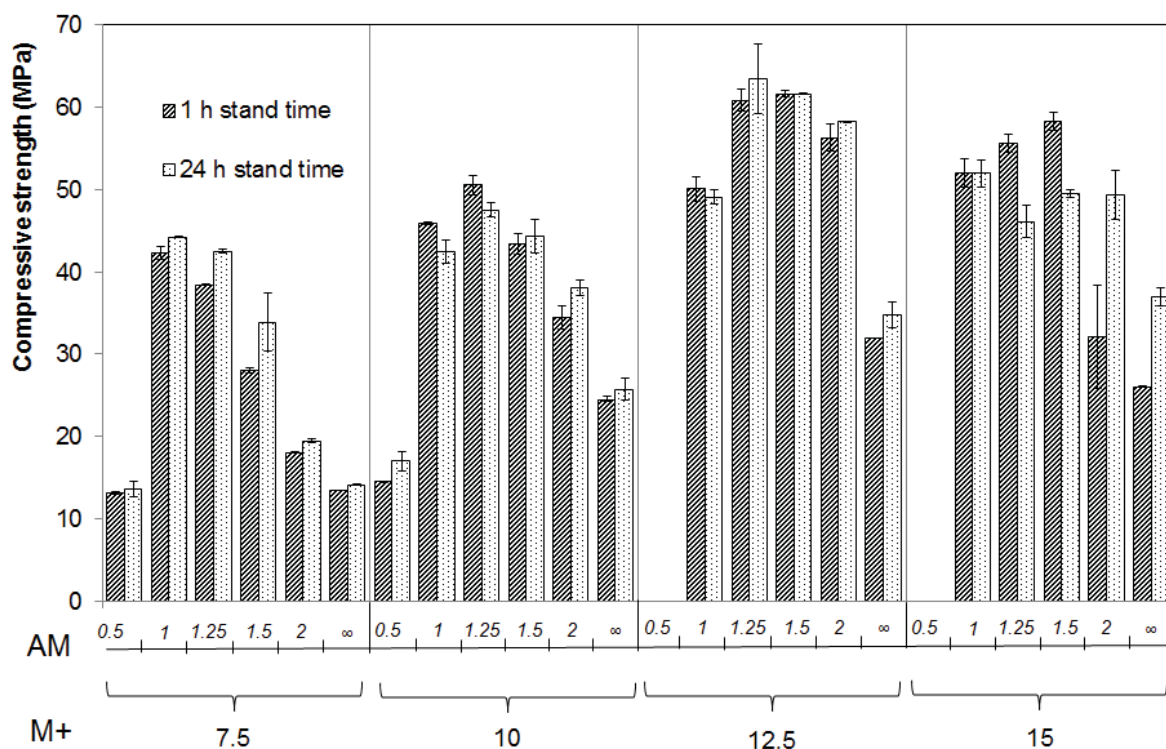


Figure 3. Compressive strengths at 28 days for 1 h and 24 h of stand time of 100% FA mortars (70°C curing temperature) for a range of alkali modulus (AM) and alkali dosage (M+). Error bars represent the range of obtained values.

3.1.2 Effect of curing temperature

Figure 4 shows the effect of curing temperature on the 28-day strengths of all mixes. It can be seen that in all cases, with the exception of those with the lowest AM (0.5), 70°C curing temperatures give significantly increased strengths compared to those cured at 50°C for the same time. The same trend was observed irrespective of the “stand time” duration. Mixes with low alkali modulus were extremely viscous and also tended to expand upon thermal curing, forming a muffin like top. Lower curing temperature leads to mitigation of such expansion and this is reflected in the increased strengths.

The observed effect of curing temperature on the mechanical strength is well documented in the literature.

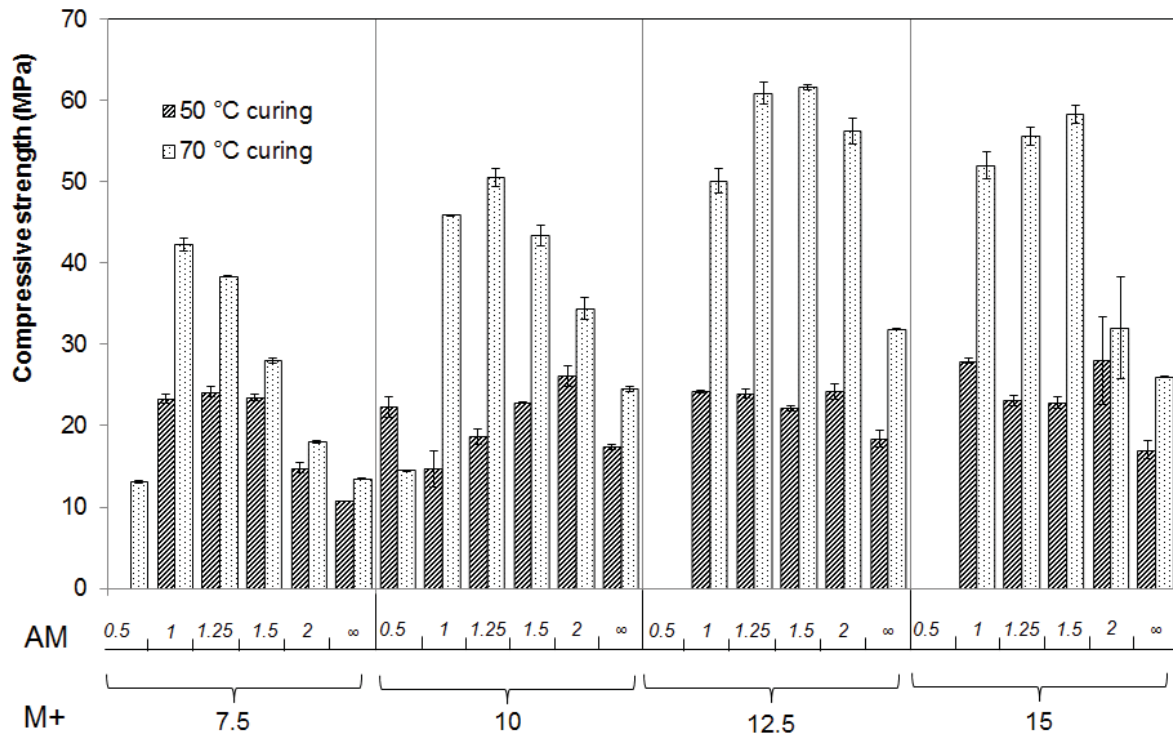
Investigations on reactivity of FA under thermal curing are reported to having been carried out for

temperatures in the range 30 °C to 85 °C [25]. Another study [26] found that increasing the curing temperature

from 45 °C to 65 °C resulted in a 5-fold rise of mechanical strength, whereas a 10-fold rise was observed

between 65 °C and 85 °C. Reaction kinetics resulting from different curing temperature were investigated with

227 isothermal calorimetric tests on different materials (Portland cement, activated slag and fly ash, and selected
 228 fly ash–slag blends) at 25 °C, 35 °C, and 40 °C, observing the development of the polymerisation [27].



229 **Figure 4.** Compressive strengths at 28 days of 100% FA mortars for 50°C and 70°C curing temperatures (1 h
 230 stand time) for a range of alkali modulus (AM) and alkali dosage (M+). Error bars represent the range of
 231 obtained values.
 232
 233

234 3.1.3 Effect of Alkali Dosage

235 The alkali dosage is a proxy for the alkali concentration, and describes the mass ratio of sodium oxide (Na₂O) in
 236 the activating solution to FA, where the water to total reactive solids ratio is fixed. An increase in alkali dosage
 237 (M+) resulted in an increase of the strength up to an M+ of 12.5%. Beyond this ‘optimum’ value, the strengths
 238 decreased, which is attributed to saturation of the gel with alkali ions resulting in less free water to be
 239 available for speciation of silica and alumina oligomers from the dissolution of FA.

240 3.1.4 Effect of Alkali Modulus

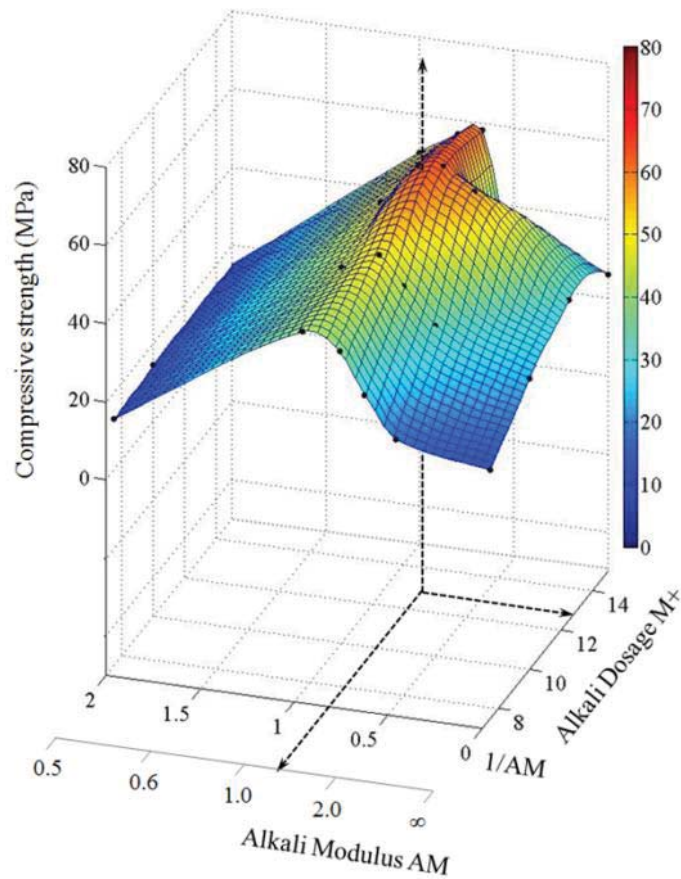
241 The alkali modulus (AM) is the mass ratio of sodium oxide to silica in the activating solution and it is a proxy for
 242 the amount of added silica in the activator solution. An optimum range of values for the alkali modulus was
 243 identified, above and below which strengths decrease. With increasing alkali dosage, that ‘sweet spot’

244 broadens out towards higher alkali modulus. Again, results for $M^+ = 15\%$ do not follow these trends. In
245 general, alkali moduli between 1 and 1.25 give the highest strengths across the alkali dosages investigated.

246 The drop-off in strength with increasing modulus is likely to be due to the reduced amount of available silica
247 that can participate in the 'reorganisation-gelation-polymerisation' steps of the geopolymer formation and
248 thus the development of a denser and more complete and long polymer chain. The reduction in strengths at
249 low modulus ($AM=0.5$: all sodium silicate) can be attributed to the reduction of the pH in the system when
250 only sodium silicate solution is used. The expansion of the cubes upon thermal curing could also have
251 contributed.

252 Figure 5 shows a 3-D plot identifying the combined effect of alkali dosage and modulus on compressive
253 strength for curing temperature of 70°C and "stand time" of 1 hour. These curing conditions were selected
254 because (a) 70°C curing temperature gave the highest compressive strengths; (b) as previously discussed, no
255 significant benefit was observed in leaving mixes for stand time longer than 1 hour.

256 The 'sweet spot' of the optimum alkali modulus and dosage combinations has a strength maximum of 70 MPa
257 at around an alkali dosage of 12.5% and alkali modulus of 1.25.



258
259

260 **Figure 5.** 3-D plot showing the combined effects of alkali dosage and modulus on the 28-day strength of 100%
261 FA mortars (1 hour at 20 °C followed by 70 °C)

262

263 3.2 Influence of physical and chemical properties of raw materials on compressive strength

264 A comprehensive characterisation of 13 different fly ashes from coal powered electricity generating stations
265 was carried out in order to investigate the suitability of different FA sources in the UK. Chemical composition,
266 mineralogical composition, grain size distribution and strengths after alkali activation were investigated.

267 All FA samples conformed to the requirements of the BS EN-450 standard [28] with regards to the
268 $\text{SiO}_2 + \text{Al}_2\text{O}_3 + \text{Fe}_2\text{O}_3$ (SAF), SO_3 , CaO, MgO, and P_2O_5 contents, whereas three FA sources (C, H, K) had LOI higher
269 than the maximum value (Category C) prescribed in [28]. Physical properties of investigated FAs are shown in
270 Table 2, whereas Table 4 summarises the 28-day compressive strengths from mortars obtained from the
271 different FA sources. It was not possible to cast cubes for testing for four of the investigated FA sources
272 because the mixes were either too dry (FA K and M) or flash setting was experienced (FA I and J). The former

273 appears to be due to the coarse nature of the FA coupled with a high LOI. The latter may have been suitable
 274 for use in concretes if the alkali activator dosage was reduced. This has not however been investigated further.

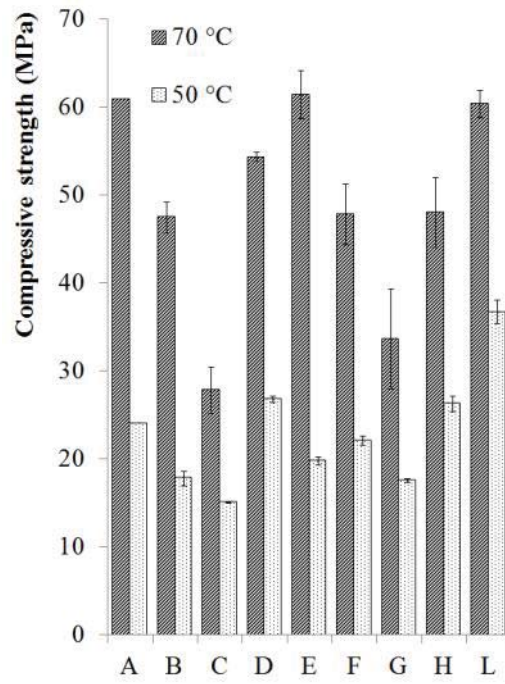
275 Optimum activator dosages were used for the geopolymer mortars, i.e. M+ 12.5% and AM 1.25. Compressive
 276 strength measured at 28 days for samples cured both at 50°C and 70°C are shown in Figure 6. The previously
 277 identified effect of curing temperature on compressive strength development was confirmed when different
 278 FA sources were investigated, with samples cured at 50°C showing lower strength than samples cured at 70°C.

279 The reaction rate of FA depends on several chemical and physical factors [9, 29]. The content of Si and Al, the
 280 amorphous phase content and the loss on ignition (LOI) are important chemical factors. Particle size of the
 281 precursor material not only affects the fresh properties (water demand, viscosity, setting time, etc.) but also
 282 affects its reactivity. The reduction of the grain size through further milling is known as mechanical activation,
 283 and it is commonly adopted for increasing the reactivity of powders [30]. The trend between compressive
 284 strength and percentage volume passing 45 µm is shown in Figure 7. The value of 45 µm was chosen according
 285 to the EN-450 [28] as indicative size for determining the fineness of the FA. The strength data were also
 286 plotted versus D_{50} , i.e. the value of the particle diameter at 50% in the cumulative distribution, and a similar
 287 trend was observed, see Figure 8. The fineness of the FA appeared therefore to correlate to the compressive
 288 strengths, whilst no relationship was observed linking the compressive strength to amorphous content, LOI, or
 289 silicon-aluminium-iron oxides (SAF) content for the investigated ashes.

290 **Table 4.** Compressive strengths for mortars produced with the 13 FA sources investigated. Values are given in
 291 MPa.

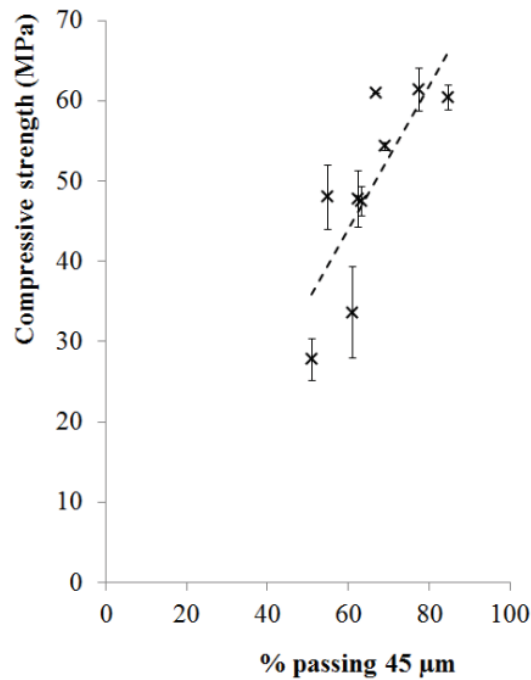
Ash source	70° curing					50° curing				
	1-day	3-day	7-day	28-day		1-day	3-day	7-day	28-day	
A	35.3	63.9	63.0	60.9		3.9	25.7	24.4	24.0	
B	31.4	52.1	43.5	45.7	49.2	4.2	17.8	18.2	18.6	16.9
C	22.4	28.5	28.6	30.4	25.2	3.6	15.3	15.1	15.1	14.9
D	41.3	63.6	60.8	53.8	54.8	7.0	20.6	24.8	26.4	27.1
E	44.1	68.2	68.1	64.1	58.7	6.9	27.0	22.2	19.3	20.2
F	27.2	50.1	43.9	51.2	44.3	4.5	18.3	23.0	21.5	22.6
G	20.1	36.4	32.3	27.9	39.3	3.4	18.9	18.6	17.7	17.3
H	29.1	52.7	51.1	52.0	44.0	6.0	21.1	24.5	27.1	25.4
I	-	-	-	-	-	-	-	-	-	-
J	-	-	-	-	-	-	-	-	-	-
K	-	-	-	-	-	-	-	-	-	-
L	50.5	62.0	63.4	61.9	58.8	10.39	23.8	40.3	38	35.4
M	-	-	-	-	-	-	-	-	-	-

292



293
 294
 295
 296
 297

Figure 6. 28-day compressive strength of 9 FA sources at different curing temperatures. Letters A-L equate to same in Table 1 and Figs. 1-2. Error bars represent the range of obtained values.



298
 299
 300

Figure 7. 28-day compressive strength of 9 FA sources cured at 70 °C vs. % volume passing 45 µm sieve. Error bars represent the range of obtained values.

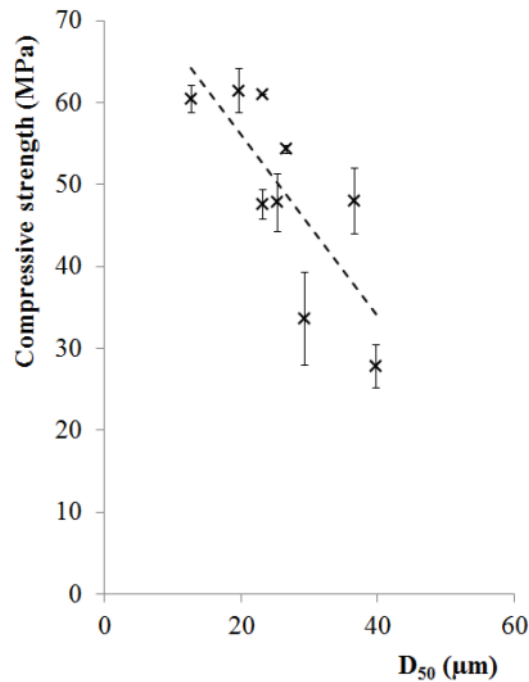


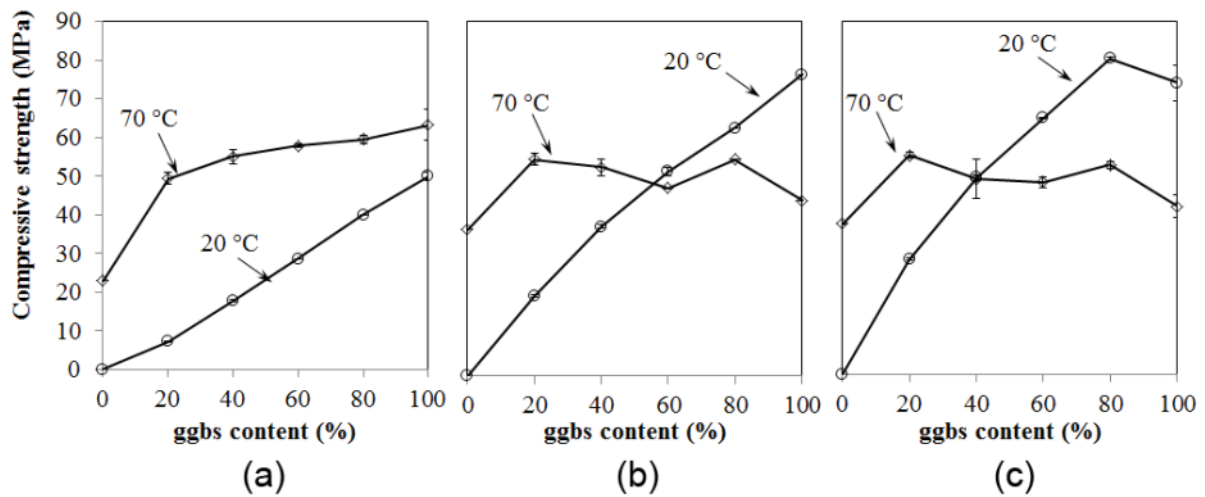
Figure 8. 28-day compressive strength of 9 FA sources cured at 70 °C vs. D₅₀. Error bars represent the range of obtained values.

301
302
303
304

305 It may therefore be concluded that one of the most important factors to consider for achieving high
306 compressive strengths is the grain size of the FA. It must, however, be emphasised that ten out of thirteen of
307 the tested FA samples are suitable for use in concretes to partially replace Portland cement and thus conform
308 to EN-450. Attempts to examine fuel ash from lagoons did not prove possible. It may be that the chemical
309 composition of lagoon ash has been altered over time and it is thus considerably different from all the sources
310 investigated in this programme of work.

311 **3.3 Effect of partial replacement of FA with ggbs**

312 Mortar mixtures containing only FA did not develop any significant strength at room temperature. However,
313 the addition of ggbs at any level gave significant strength enhancements even at room temperature. Figure 9
314 shows the strength of FA/ggbs based mortars with M+ 7.5% and AM 1.25. There is an almost linear
315 relationship between the amount of ggbs in the binder and the strength at 1, 7 and 28 days where cubes were
316 cured at room temperature (20°C). This seems to suggest that FA did not contribute much to the strength.
317 There was a significant increase in the strength from ~20MPa to ~50MPa with the addition of only 20% ggbs
318 when cured for 1 day at 70 °C. Higher levels of ggbs cured for 1 day resulted in smaller incremental increases
319 up to ~60MPa at 100% ggbs.

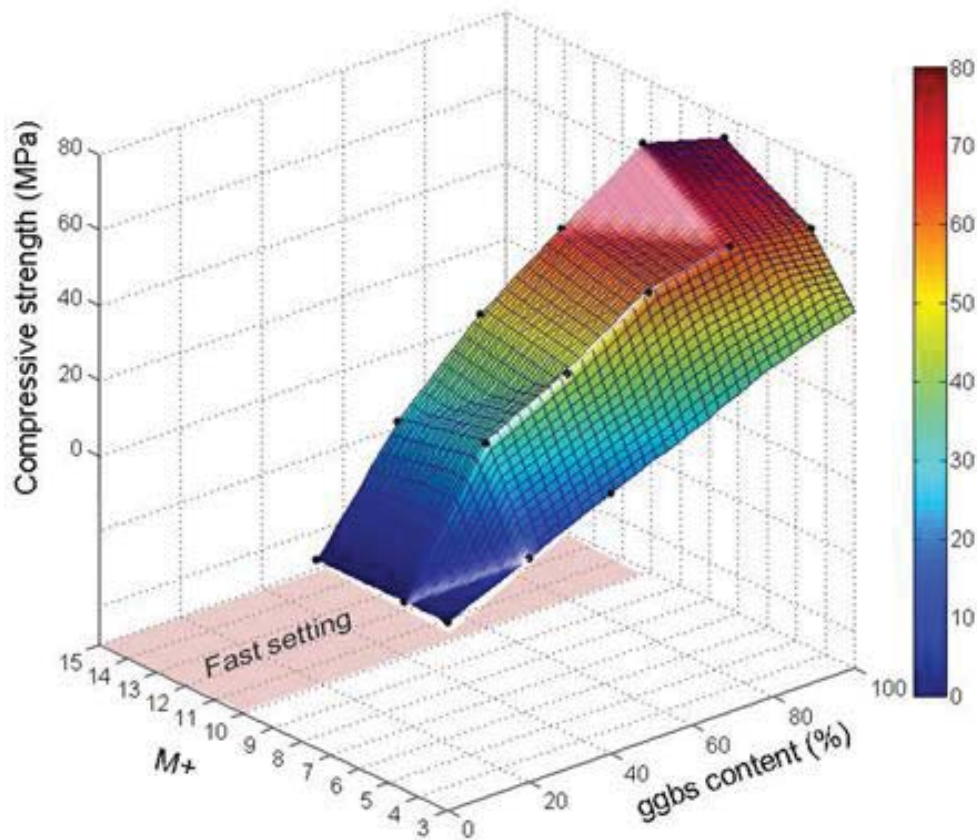


320
 321 **Figure 9.** Effect of ggbs substitution rate on the strength of sodium silicate/sodium hydroxide-activated binders
 322 with M+ 7.5% and AM 1.25. (a) 1 day; (b) 7 days; (c) 28 days. Error bars represent the range of obtained values.
 323

324 Continued curing at 70°C for 7 and 28 days resulted in strength reductions for mixes with greater than 20%
 325 ggbs. This is believed to be due to self-desiccation and resulting drying shrinkage, which is an effect that has
 326 previously been observed in alkali-activated slags [7]. In accordance with this effect, the highest strength was
 327 achieved for specimens cured at room temperature and not for oven-cured samples. Compressive strength of
 328 80 MPa was obtained at 28 days for the mortar containing 80% slag and cured at room temperature.

329 Subsequent investigations focussed on the effect of alkali dosage on the strength development of FA/ggbs
 330 blends. The AM was kept constant while the M+ was varied from 3% to 10% for varying levels of FA
 331 replacement with ggbs. Figure 10 shows the 3-D plot of the 28-day compressive strength of specimens cured
 332 at room temperature. M+ 10% mixes could not be easily cast for ggbs contents higher than 20% due to quick
 333 setting. It can be observed that the increase in ggbs content led to an incremental increase in the compressive
 334 strength.

335



336
 337 **Figure 10.** 3-D plot showing the combined effects of FA/ggbs ratio and M+ variation on the 28-day compressive
 338 strength of sodium silicate/sodium hydroxide-activated binders cured at room temperature
 339

340 **3.4 X-Ray Diffraction results for raw materials and reacted pastes**

341 In order to investigate the nature and composition of the reaction products, raw material and reacted pastes
 342 were analysed with X-ray diffraction (XRD) technique. FA A was used for the pastes. The raw materials were
 343 activated with the following dosages: M+ 7.5%, AM = 1.25 and w/s ratio 0.37. 100% FA, 100% ggbs and a 50/50
 344 FA/ggbs paste were produced. After 28 days oven curing at 70 °C, pastes were crushed using distilled water in
 345 a McCrone Mill for 5 min and dried at 50°C for 14 hours. An internal standard (zincite, ZnO) was included at
 346 10% in weight for semi-quantitative analysis of the material composition. Diffractograms for unreacted FA
 347 showed approximately 75% of amorphous content, due to the inclusion of the internal standard. After
 348 depuration from the 10% zincite, the main crystalline phases were quartz (SiO₂, 3.9% in weight), mullite
 349 (2Al₂O₃·SiO₂, 10.6% in weight), and minor contents of calcite (CaCO₃, 1.4% in weight) and maghemite (Fe₂O₃,
 350 0.8% in weight), whereas the amorphous content was around 83%, in line with the value shown in table 2.
 351 Ggbs sample with internal standard showed an amorphous content of about 88%, which resulted in about 98%

352 after depuration from the 10% crystalline ZnO, with about 1.7% in weight of crystalline CaCO₃ and traces of
353 quartz.

354 Figure 11 shows the compared diffractograms for 100% FA (A), 100% ggbs (B) and 50/50 FA/ggbs (C).

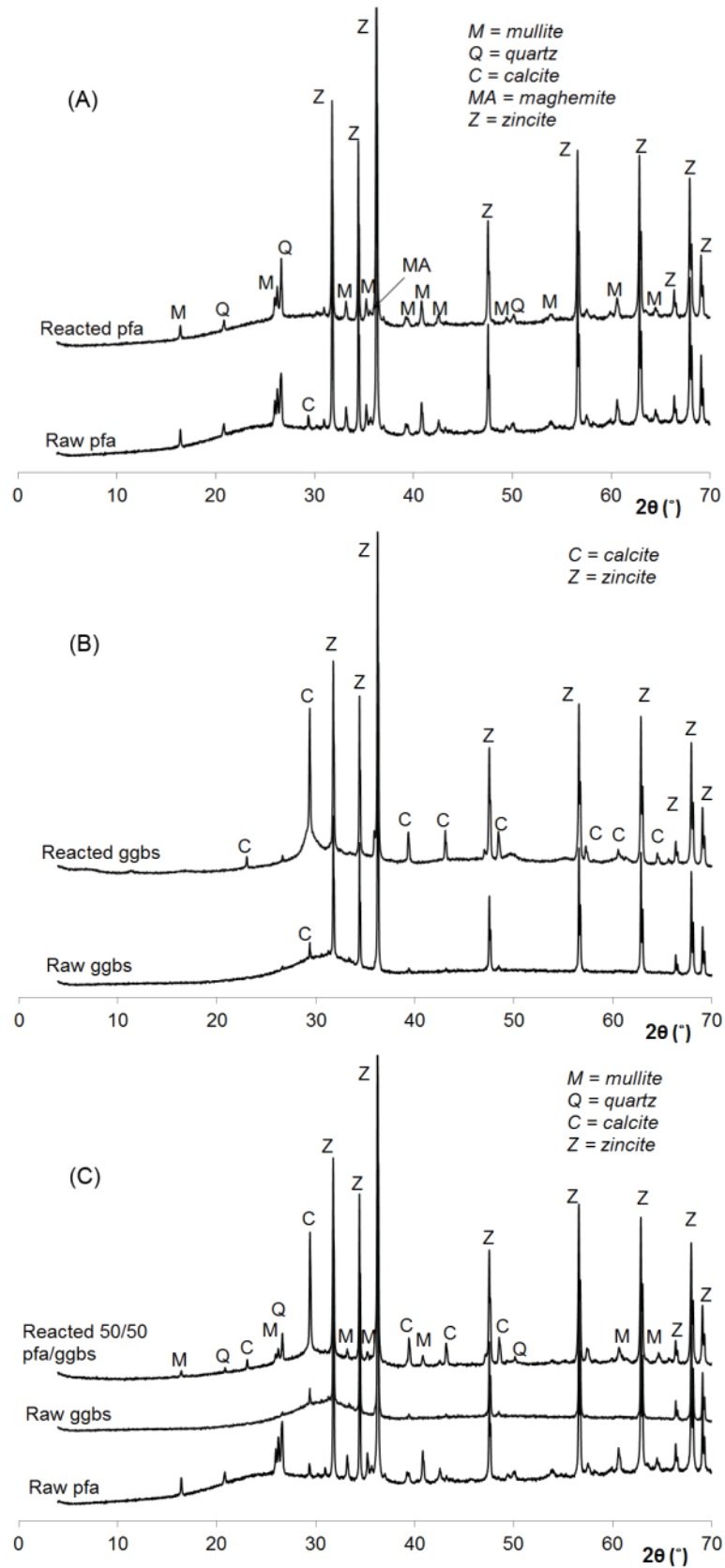


Figure 11. XRD diffractograms of raw materials and reacted pastes. (a) 100% FA (b) 100% ggbs (c) 50/50 FA/ggbs

355
356
357
358

359 No new crystalline phase was obtained from the activation of FA. Quartz and mullite, as expected, did not
360 participate to the reaction, as their mass contents remained almost unchanged. On the contrary, the activation
361 of ggbs resulted in a decrease in amorphous content from 98% to 87% (corrected values) and in an increase in
362 calcite content from 1.7% to 9.4%, with peaks for calcite clearly higher in the activated ggbs paste
363 diffractogram. It is likely that the calcite in activated ggbs sample is a combination of high and low crystallinity
364 forms, as apparent by the broad base to the $29.4^{\circ}2\theta$ peak.

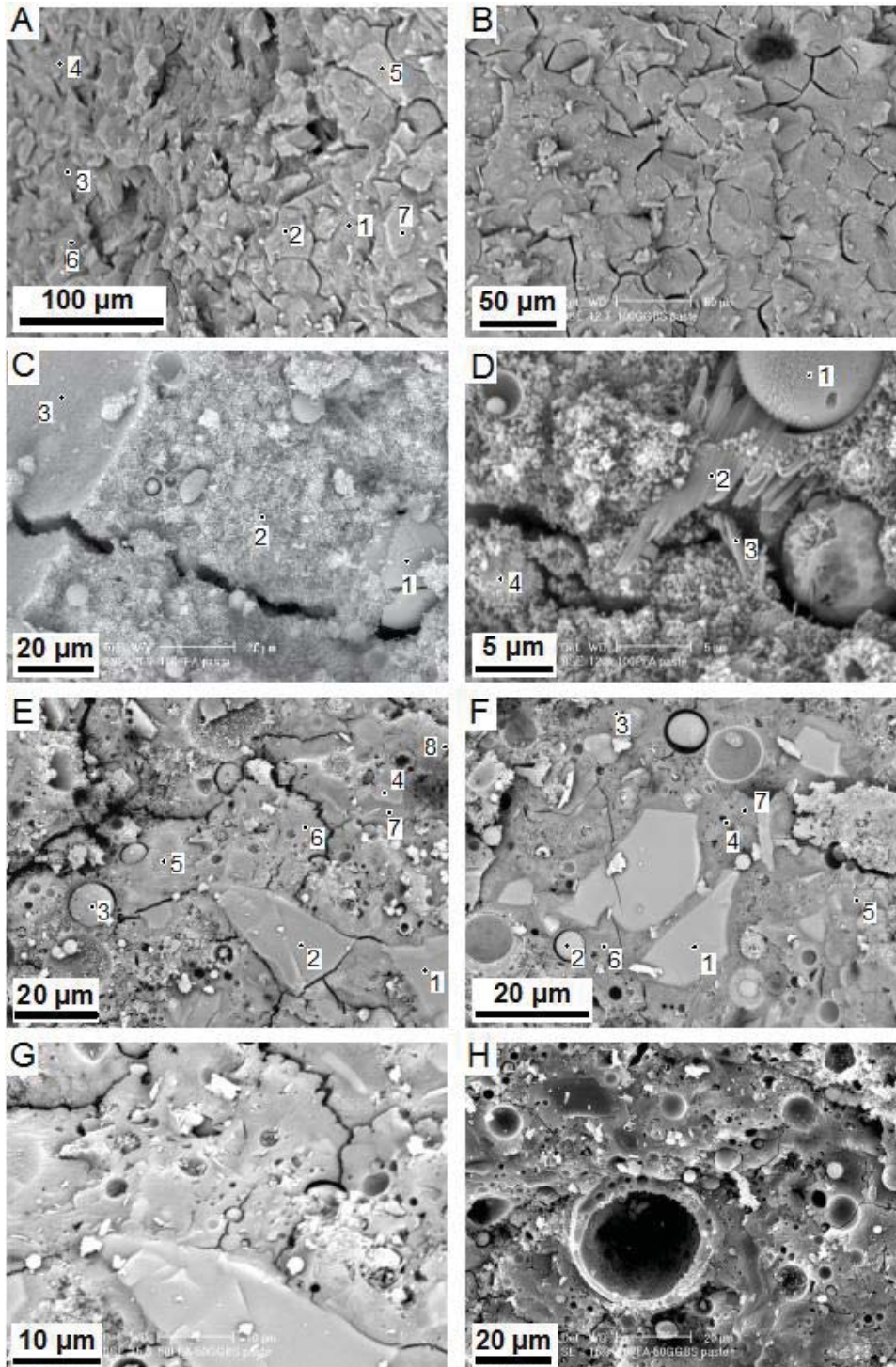
365 The 50/50 FA/ggbs paste produced results half way between 100% ggbs and 100% FA pastes. Quartz and
366 content did not change, whereas crystalline calcite content increased from 1.5 wt% of the starting material to
367 6.0 wt% of the paste, with the amorphous phase decreasing from 90.7% to 88 wt%.

368 **3.5 Microstructure and chemistry of the pastes**

369 The different mechanical behaviour of FA and FA/ggbs mixes discussed above would be expected to correlate
370 in some way with microstructure or reaction products found in the pastes. To test this, SEM analysis was
371 carried out on the three pastes, i.e. 100% ggbs, 100% FA and 50/50 FA/ggbs, cured at 70°C for 28 days.

372 *3.5.1 100% ggbs paste*

373 The basic microstructure of 100% ggbs paste is shown in Figure 12(a) and (b). The paste is made up of
374 unreacted particles of ggbs in a smooth and homogenous looking gel. The paste is traversed by
375 interconnecting curved fractures that locally break up the paste into $\sim 10\text{-}20\ \mu\text{m}$ size conchoidal particles. The
376 fractures have morphologies characteristic of desiccation, particularly evident in Figure 12(b). EDS-based
377 chemical analysis of unreacted ggbs and the surrounding gel from the points indicated in Figure 12(a) are
378 summarised in Table 5 and on the ternary diagram in Figure 13. The vertices of the ternary diagram have been
379 chosen to encompass the main chemical compositions of the gels developed in all three pastes. The Na, Ca and
380 Al values in Table 5 have been 'normalised' to Si content in each case in order to alleviate the inherent semi-
381 quantitative nature of EDS chemical analysis on rough surfaces. It is worth noting in Figure 13 that the
382 unreacted 100% ggbs particles and the 100% ggbs gel form separate clusters that lie on a line that intersects
383 the Na/Si corner of the plot (see dashed line in Figure 13). The 100% ggbs gel thus lies about half way along a
384 potential mixing line between the original ggbs composition and the activator composition, suggesting more or
385 less equal contribution of ggbs and activator in the reaction to produce the gel.



386
 387
 388
 389
 390
 391
 392
 393
 394
 395

Figure 12. SEM back-scattered electron (A-G) and secondary electron (H) images of geopolymer paste broken surfaces. Numbered spots on A, C, D, E and F are locations of EDS chemical analyses. A & B: paste made with 100% ggbs. C&D: paste made with 100% FA. E-H: paste made with 50% ggbs and 50% FA.

Table 5. EDS analysis of 100% ggbs paste. Spot numbers refer to Figure 14(a). Analyses with Oxford Instruments INCA.

Spot	O	Na	Mg	Al	Si	K	Ca	Ti	Mn	Fe	Al/Si	Ca/Si	Na/Si	Description
------	---	----	----	----	----	---	----	----	----	----	-------	-------	-------	-------------

1	53.42	20.99	2.00	3.22	9.96	0.15	9.95	0.13	0.17		0.323	0.999	2.107	C-(N)-A-S-H gel
2	50.95	16.29	3.13	4.03	11.07	0.31	13.69	0.27	0.23		0.405	1.237	1.472	C-(N)-A-S-H gel
3	46.93	20.21	1.07	3.00	11.38	0.42	16.63	0.23			0.301	1.461	1.776	C-(N)-A-S-H gel
4	49.80	19.25	1.38	3.18	11.25	0.27	14.20	0.23	0.28	0.16	0.319	1.262	1.711	C-(N)-A-S-H gel
5	43.54	5.30	3.60	5.80	15.09	0.41	25.23	0.28	0.60		0.582	1.672	0.351	Unreacted ggbs particle
6	43.57	7.08	3.65	4.94	13.72	0.53	24.72	0.60	1.05		0.496	1.802	0.516	Unreacted ggbs particle
7	36.59	3.71	3.14	5.22	15.97	0.61	33.99	0.56	0.56		0.524	2.128	0.232	Unreacted ggbs particle

396

397 **Table 6(a).** EDS analysis of 100% FA paste. Spot numbers refer to Figure 14(c). Analyses with Oxford
398 Instruments INCA.

Spot	O	Na	Mg	Al	Si	K	Ca	Ti	Mn	Fe	Al/Si	Ca/Si	Na/Si	Description
1	47.27	2.78	0.76	15.02	26.5	3.58	0.94	0.78		2.36	1.508	0.035	0.105	Unreacted FA particle
2	54.2	8.53	0.54	11.15	19.08	1.51	2.08	0.28		2.62	1.119	0.109	0.447	N-A-S-H gel
3	49.77	10.24	0.58	8.96	22.88	2.18	2.7	0.51		2.17	0.900	0.118	0.448	N-A-S-H gel

399

400 **Table 6(b).** EDS analysis of 100% FA paste. Spot numbers refer to Figure 14(d). Analyses with Oxford
401 Instruments INCA.

Spot	O	Na	Mg	Al	Si	K	Ca	Ti	Mn	Fe	Al/Si	Ca/Si	Na/Si	Description
1	53.09	1.21	0.89	14.18	23.50	2.89	1.34	0.44		2.37	1.424	0.057	0.051	Unreacted FA particle
2	47.03	14.67	0.53	9.57	20.68	1.94	1.72	0.42	0.23	3.20	0.961	0.083	0.709	N-A-S crystal
3	48.34	18.89	0.49	7.77	17.44	1.93	1.63	0.53		3.03	0.780	0.093	1.083	N-A-S crystal
4	51.39	7.02	0.76	11.05	21.23	1.93	2.11	1.18		3.29	1.109	0.099	0.331	N-A-S-H gel

402

403 **Table 7(a).** EDS analysis of 50/50 FA/ggbs paste (1st sample). Spot numbers refer to Figure 14(e). Analyses with
404 Oxford Instruments INCA.

Spot	O	Na	Mg	Al	Si	K	Ca	Ti	Mn	Fe	Si/Al	Ca/Si	Na/Si	Description
1	38.00	0.27	4.86	6.98	18.58	0.51	29.44	0.63	0.46	0.26	0.701	1.584	0.015	Unreacted ggbs particle
2	29.37	0.37	4.41	7.49	19.39	0.51	37.24	0.61	0.39	0.23	0.752	1.921	0.019	Unreacted ggbs particle
3	45.51	1.25	1.17	18.27	24.38	2.19	1.22	0.64		5.39	1.834	0.050	0.051	Unreacted FA particle
4	40.95	0.47	4.53	6.95	17.02	0.47	28.54	0.40	0.32	0.37	0.698	1.677	0.027	Unreacted ggbs particle
5	49.12	8.41	1.21	7.04	20.92	1.28	10.44	0.39		1.06	0.707	0.499	0.402	C-(N)-A-S-H gel
6	48.95	5.10	2.83	6.42	17.77	1.03	16.37	0.31	0.38	0.87	0.645	0.921	0.287	C-(N)-A-S-H gel
7	40.81	5.41	2.20	6.96	21.86	1.55	19.17	0.44	0.49	1.12	0.699	0.877	0.247	C-(N)-A-S-H gel
8	39.53	6.31	1.93	8.45	23.71	1.55	15.8	0.39	0.5	1.84	0.848	0.666	0.266	C-(N)-A-S-H gel

405

406

407

408 **Table 7(b).** EDS analysis of 50%/50% FA/ggbs paste (2nd sample). Spot numbers refer to Figure 14(f). Analyses
409 with Bruker Quantax 70.

Spot	O	Na	Mg	Al	Si	K	Ca	Ti	Mn	Fe	Si/Al	Ca/Si	Na/Si	Description
------	---	----	----	----	----	---	----	----	----	----	-------	-------	-------	-------------

1	44.01	1.20	4.42	6.33	17.39	0.52	24.98	0.46	0.55	0.13	0.636	1.436	0.069	Unreacted ggbs particle
2	44.37	3.06	1.19	16.12	26.12	3.51	2.16	0.37		3.10	1.618	0.083	0.117	Unreacted FA particle
3	51.08	7.82	1.08	6.88	18.22	1.85	12.79	0.27			0.691	0.702	0.429	C-(N)-A-S-H gel
4	49.55	7.53	0.86	7.16	18.21	2.14	12.67	0.57	0.41	0.89	0.719	0.696	0.414	C-(N)-A-S-H gel
5	46.36	8.01	1.54	7.12	20.92	0.96	13.64	0.24		1.20	0.715	0.652	0.383	C-(N)-A-S-H gel
6	49.03	8.32	1.78	7.18	20.29	2.05	10.17	0.29	0.25	0.65	0.721	0.501	0.410	C-(N)-A-S-H gel
7	51.84	7.97	1.54	5.95	17.14	1.54	12.17		0.89	0.97	0.597	0.710	0.465	C-(N)-A-S-H gel

410

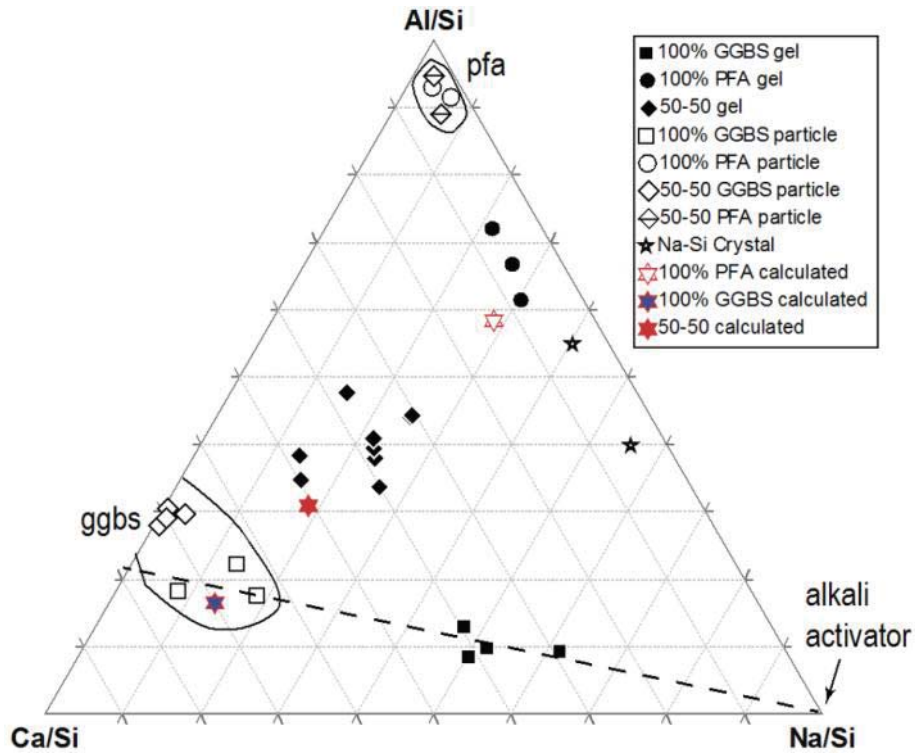
411 3.5.2 100% FA paste

412 The basic microstructure of 100% FA paste is shown in Figure 12(c) and (d). The paste is made up of unreacted
413 particles of FA in a rough and sugary looking granular gel. There are commonly gaps between the gel and the
414 unreacted FA suggesting weak bonding of gel to unreacted particles. Some long fractures are present, but
415 these have a morphology suggesting they formed during breakage of the sample rather than by desiccation.
416 EDS-based chemical analysis of unreacted FA and the surrounding gel from the points indicated in Figure 12(c)
417 and (d) are summarised in Table 6(a) and (b) as well as on the ternary diagram in Figure 13. It is clear that the
418 FA cenospheres are relatively enriched in Al and depleted in Ca and Na relative to Si content. On the other
419 hand, the rough sugary gel is relatively enriched in Na and slightly enriched in Ca relative to the unreacted FA.
420 In this case, the unreacted FA and the gel do not lie directly on a potential mixing line between the unreacted
421 FA and the Na/Si corner of Figure 13. While this may be due to analytical errors resulting from EDS-analysis of
422 rough surfaces, it is also possible that reactions responsible for gel formation preferentially fractionated
423 available Ca in the FA into the gel.

424 3.5.3 50% FA and 50% ggbs paste

425 The basic microstructure of 50% FA and 50% ggbs paste is shown in Figure 12(e) and (f). The paste is made up
426 of unreacted particles of FA and ggbs in a smooth homogeneous looking gel. The microstructure for 50/50
427 FA/ggbs shows unreacted or partially reacted FA cenospheres and ggbs grains surrounded by an amorphous
428 matrix which was smooth and homogeneous in some places whilst rough and more heterogeneous in others.
429 There are relatively few fractures, which do not look like desiccation fractures. The contact between gel and
430 unreacted ggbs is typically sharp, whereas there is often a gap between the gel and unreacted FA cenospheres;
431 the large cenosphere in the centre of Figure 12(h) is an exception. EDS-based chemical analysis of unreacted
432 FA/ggbs and the surrounding gel from the points indicated in Figure 12(e) and (f) are summarised in Table 7(a)
433 and (b) as well as on the ternary diagram in Figure 13. The unreacted ggbs and FA have compositions similar to

434 those in the 100%ggbs and 100%FA pastes, respectively (Figure 13). The gel has a composition that lies within
 435 a triangle formed by the unreacted FA and ggbs and the alkali-activator composition indicating all three
 436 reactants were involved in the reaction to produce the gel. The position of the gel composition relative to the
 437 reactants indicates ggbs was the main contributor to the gel and the alkali activator the least.



438
 439 **Figure 13.** Triangular plot of Ca, Al, Na compositions normalised to Si content for FA and GGBS particles,
 440 various gels, and some Na-Si crystals formed in one sample. Calculated compositions for the pastes are plotted
 441 as six pointed stars. Added NaOH and sodium silicate solution would plot on the Na/Si corner. See text for
 442 further explanation and discussion.
 443

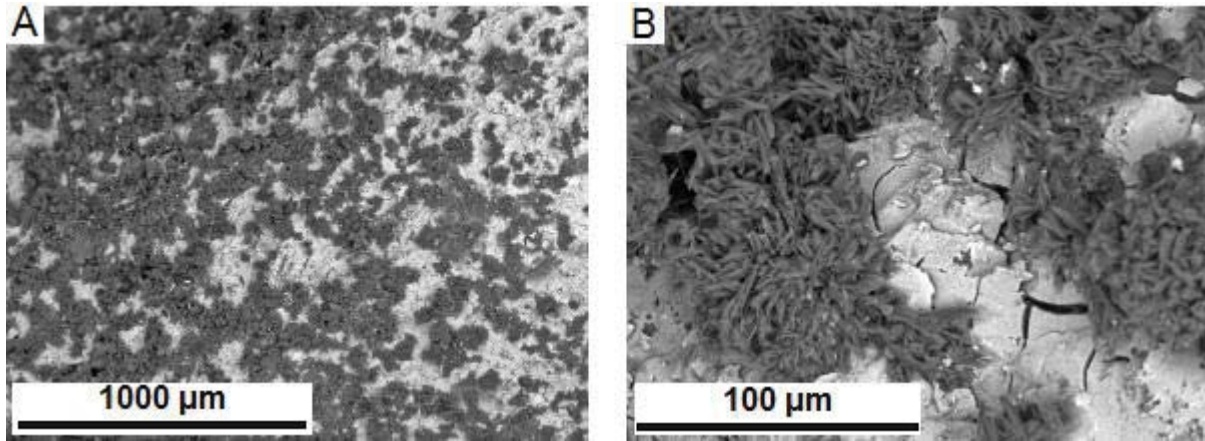
444 The three microstructures are quite different. The 100% FA gel looks granular and potentially porous with a
 445 commonly poor adhesion to unreacted FA particles. In contrast the 100% ggbs gel is homogeneous and looks
 446 denser, but is cut by interconnecting desiccation cracks. Both microstructures look inherently weak. The
 447 50%FA-50%ggbs gel microstructure is homogeneous and dense looking and lacks the desiccation cracks found
 448 in the 100% ggbs gel. The addition of aluminium from the FA has resulted in a non-granular gel that does not
 449 shrink, and is perhaps stronger.

450 Overall, the main product from a FA-based system is a sodium-alumina-silicate-hydrate geopolymeric gel (N-A-
 451 S-H) with very low Ca/Si ratio, though perhaps a little higher than would be expected from the compositions of

452 FA and the alkali activator. The gel composition is similar to the calculated bulk composition of the gel
453 ingredients (Figure 13).

454 In contrast, the high calcium 100% ggbs system produces a calcium-alumina-silicate-hydrate gel (C-A-S-H) with
455 low Al/Si ratio of 0.3-0.4 and a Ca/Si of 1 to 1.5, as has been reported by several researchers [31-33] for alkali
456 activated slag systems. The reaction products are similar to the C-S-H gel in Portland cement systems, where
457 higher Ca/Si ratios are obtained in the range 1.2 to 2.3 [34], and are presumably various forms of calcium
458 silicate hydrates and calcium aluminium hydrates. The gel composition is much more Na-rich than the
459 calculated bulk composition of the gel ingredients and even the unreacted ggbs particles contain significant Na
460 (Figure 13). Re-examination of the same surface about 9 months later revealed a coating of sodium carbonate
461 crystals in rosette forms (Figure 14) indicating an excess of Na in the gel reaction. These rosettes were not
462 visible shortly after the 100% ggbs paste was made (see Figure 12(a) and (b)). This raises the possibility that
463 the higher than expected Na measurements from the surfaces in Figure 12 (a) and (b) reflect initial sub-
464 microscopic formation of sodium carbonate crystals at the sample surface as efflorescence due to evaporation
465 of excess sodium-bearing solute, which as it progressed led to formation of the larger rosette crystals. Thus, it
466 is suggested that the 100% ggbs gel at the broken sample surface has progressively incorporated Na from the
467 alkali activator.

468 The 50% FA 50% ggbs system produces a C-A-S-H gel with Na/Si in the range 0.25-0.5, Ca/Si at 0.5-0.9 and Si/Al
469 at 0.6-0.85, compositions similar to the calculated bulk composition of the gel ingredients (Figure 13). The gel
470 microstructure looks dense and is uncracked. It has been reported in [35] that alkalis (Na in this case) can be
471 incorporated into a C-A-S-H gel structure in order to balance the charge of tetrahedral Al, therefore it could
472 also be written C-(N)-A-S-H. As suggested in the literature [36], the calcium silicate hydrate gel fills the pores
473 and voids left by the water escaping the "pure" geopolymeric gel (N-A-S-H), resulting in a more compact and
474 dense structure that is responsible for the increase in mechanical strength compared to the 100% pfa paste.
475 The coexistence of N-A-S-H and C-A-S-H gels has been reported in the literature [33, 36-37].



476
 477 **Figure 14.** Back-scattered electron images of 100% ggbs paste surface ~9 months after images in Figure 12. A
 478 shows distribution of sodium carbonate crystals (dark areas) grown on the paste surface (light area). B shows a
 479 detail of the rosette structure formed by the sodium carbonate crystals and the characteristic desiccation
 480 cracks in the gel.
 481

482 **4 Conclusions**

483 Geopolymer and alkali activated binders can offer a possible alternative to Portland cement concrete.
 484 Notwithstanding all the research work that has been carried out all over the world, an easy way of selection of
 485 raw material and their proportioning to obtain desired properties has remained a trial and error procedure.
 486 The following factors affecting the mechanical properties were therefore investigated in order to provide
 487 guidance for the selection of raw materials and their proportioning to produce geopolymer concretes of the
 488 required properties: (a) the effect of curing procedure and activator dosages on the strength of FA-based
 489 mortar; (b) the influence of physical and chemical properties of different FA sources; (c) the effect of partial FA
 490 replacement with ggbs.

491 The conclusions from this work are:

- 492 1. Curing temperature has a very significant effect on strength of FA based geopolymers: specimens
 493 cured at 70°C were considerably stronger than specimens cured at 50°C. Stand time was found to be
 494 less important and as such an 1 hour stand time before oven curing was considered sufficient.
- 495 2. The dosage of activators is very important for not only achieving the required early age properties but
 496 also for the effect on compressive strength. A 'sweet spot' of the optimum alkali modulus and dosage
 497 combinations, i.e. alkali dosage of 12.5% and alkali modulus of 1.25, gave compressive strength of ~70
 498 MPa.

- 499 3. Physical and chemical properties of potential FA sources should be investigated before selecting the
500 most suitable one. Average grain size was found to be one of the important factors affecting the
501 potential compressive strength. Coarse FA coupled with low amorphous content and high LOI needs
502 to be avoided.
- 503 4. Partial FA replacement with ggbs leads to increases in the compressive strength. Strengths of 80 MPa
504 with only M+ 7.5% and AM 1.25 were obtained. The other benefit from such blends is that curing at
505 room temperature only is sufficient and no elevated curing temperatures are needed.
- 506 5. SEM investigation on pastes of 100% FA, 100% ggbs and 50/50 FA/ggbs assisted in determining the
507 microstructure, reaction products and their chemical composition. The 100% FA and 100% ggbs mixes
508 produce distinctly different microstructures, i.e. dominated by coarse granularity and desiccation
509 cracking respectively. The 50/50 FA/ggbs mix develops a homogeneous, dense gel with little
510 microcracking and good bonding to unreacted ggbs and FA particles. The 50/50 FA/ggbs
511 microstructure looks like it should be stronger and it has been proved to be so when 70° C oven curing
512 conditions are applied.
- 513 6. A calcium alumina silicate hydrate gel with inclusions of Na⁺ cations in the structure was found in the
514 samples containing ggbs. This was denser than the sodium alumina silicate hydrate gel (N-A-S-H)
515 found for 100% FA samples and this could explain the improved compressive strengths.

516 **5 Acknowledgements**

517 This research was carried out at the University of Liverpool in the framework of the Carbon Trust Applied
518 Research Grant 0911-0252 “Ultra High Performance Fibre Reinforced Cementless Precast Concrete Products”.
519 The work was then continued at Queen’s University of Belfast with the financial support of the SUSCON
520 project, which has received funding from the European Union Seventh Framework Programme (FP7/2007-
521 2013) under Grant Agreement No. 285463 (Call FP7-2011-NMP ENV-ENERGY-ICT-EeB).

522 **6 References**

- 523 [1] Davidovits, J. (2008) Geopolymer chemistry and applications. Institut Geopolymere.

- 524 [2] Davidovits, J. (1989). Geopolymers and geopolymeric materials. *Journal of thermal analysis*, 35(2),
525 429-441.
- 526 [3] Davidovits, J. (1991). Geopolymers. *Journal of thermal analysis*, 37(8), 1633-1656.
- 527 [4] Davidovits, J. (1993). Geopolymer cements to minimise carbon-dioxide greenhouse-warming. *Ceram.*
528 *Trans.*, 37, 165-182.
- 529 [5] Barbosa, V. F., MacKenzie, K. J., & Thaumaturgo, C. (2000). Synthesis and characterisation of materials
530 based on inorganic polymers of alumina and silica: sodium polysialate polymers. *International Journal*
531 *of Inorganic Materials*, 2(4), 309-317.
- 532 [6] Kriven, W. M., Bell, J. L., & Gordon, M. (2003). Microstructure and Microchemistry of Fully-Reacted
533 Geopolymers and Geopolymer Matrix Composites. *Advances in Ceramic Matrix Composites IX*,
534 *Volume 153*, 227-250.
- 535 [7] Shi, C., Roy, D., & Krivenko, P. (2006). *Alkali-activated cements and concretes*. CRC press.
- 536 [8] Van Jaarsveld, J. G. S., & Van Deventer, J. S. J. (1999). Effect of the alkali metal activator on the
537 properties of fly ash-based geopolymers. *Industrial & Engineering Chemistry Research*, 38(10), 3932-
538 3941.
- 539 [9] Provis, J. L., van Deventer, J. S. (2014). *Alkali Activated Materials*. J. L. Provis (Ed.). Springer.
- 540 [10] Jimenez, A. M. F., Lachowski, E. E., Palomo, A., & Macphee, D. E. (2004). Microstructural
541 characterisation of alkali-activated PFA matrices for waste immobilisation. *Cement and Concrete*
542 *Composites*, 26(8), 1001-1006.
- 543 [11] Kong, D. L., & Sanjayan, J. G. (2010). Effect of elevated temperatures on geopolymer paste, mortar
544 and concrete. *Cement and Concrete Research*, 40(2), 334-339.
- 545 [12] Wallah, S. E., & Rangan, B. V. (2006). Low-calcium fly ash-based geopolymer concrete: long-term
546 properties. *Res. Report-GC2, Curtin University, Australia*. pp, 76-80.
- 547 [13] Duxson, P., Fernández-Jiménez, A., Provis, J. L., Lukey, G. C., Palomo, A., & Van Deventer, J. S. J.
548 (2007). Geopolymer technology: the current state of the art. *Journal of Materials Science*, 42(9), 2917-
549 2933.
- 550 [14] Andini, S., Cioffi, R., Colangelo, F., Grieco, T., Montagnaro, F., & Santoro, L. (2008). Coal fly ash as raw
551 material for the manufacture of geopolymer-based products. *Waste management*, 28(2), 416-423.

- 552 [15] Duxson, P., Provis, J. L., Lukey, G. C., & Van Deventer, J. S. (2007). The role of inorganic polymer
553 technology in the development of 'green concrete'. *Cement and Concrete Research*, 37(12), 1590-
554 1597.
- 555 [16] Soutsos, M.N., Vinai, R., & Rafeet, A. (2015). Effect of alkali dosage and modulus on strength
556 development and microstructure of alkali-activated binders. *14th International Congress on the
557 Chemistry of Cement (ICCC 2015)*, 13-16 October 2015, Beijing, China
- 558 [17] Department of Energy & Climate Change, Electricity: chapter 5, Digest of United Kingdom energy
559 statistics (DUKES). [https://www.gov.uk/government/statistics/electricity-chapter-5-digest-of-united-](https://www.gov.uk/government/statistics/electricity-chapter-5-digest-of-united-kingdom-energy-statistics-dukes)
560 [kingdom-energy-statistics-dukes](https://www.gov.uk/government/statistics/electricity-chapter-5-digest-of-united-kingdom-energy-statistics-dukes). Accessed on 17 June 2015.
- 561 [18] Heath, A., Paine, K., Goodhew, S., Ramage, M., & Lawrence, M. (2013). The potential for using
562 geopolymer concrete in the UK. *Proceedings of the Institution of Civil Engineers: Construction
563 Materials*, 166(4), 195-203.
- 564 [19] Puertas, F., & Fernández-Jiménez, A. (2003). Mineralogical and microstructural characterisation of
565 alkali-activated fly ash/slag pastes. *Cement and Concrete composites*, 25(3), 287-292.
- 566 [20] Puertas, F., Martínez-Ramírez, S., Alonso, S., & Vazquez, T. (2000). Alkali-activated fly ash/slag
567 cements: strength behaviour and hydration products. *Cement and Concrete Research*, 30(10), 1625-
568 1632.
- 569 [21] Puligilla, S., & Mondal, P. (2013). Role of slag in microstructural development and hardening of fly ash-
570 slag geopolymer. *Cement and Concrete Research*, 43, 70-80.
- 571 [22] Ismail, I., Bernal, S. A., Provis, J. L., San Nicolas, R., Hamdan, S., & van Deventer, J. S. (2014).
572 Modification of phase evolution in alkali-activated blast furnace slag by the incorporation of fly ash.
573 *Cement and Concrete Composites*, 45, 125-135.
- 574 [23] Kumar, S., Kumar, R., & Mehrotra, S. P. (2010). Influence of granulated blast furnace slag on the
575 reaction, structure and properties of fly ash based geopolymer. *Journal of Materials Science*, 45(3),
576 607-615.
- 577 [24] British Standards Institution, Testing fresh concrete - Part 5: Flow table test, BS EN 12350-5:2000.
- 578 [25] Kovalchuk, G., Fernández-Jiménez, A., & Palomo, A. (2007). Alkali-activated fly ash: effect of thermal
579 curing conditions on mechanical and microstructural development—Part II. *Fuel*, 86(3), 315-322.

- 580 [26] Palomo, A., Alonso, S., Fernandez-Jiménez, A., Sobrados, I., & Sanz, J. (2004). Alkaline activation of fly
581 ashes: NMR study of the reaction products. *Journal of the American Ceramic Society*, 87(6), 1141-
582 1145.
- 583 [27] Chithiraputhiran, S., & Neithalath, N. (2013). Isothermal reaction kinetics and temperature
584 dependence of alkali activation of slag, fly ash and their blends. *Construction and Building Materials*,
585 45, 233-242.
- 586 [28] British Standards Institution, Fly ash for concrete. Definitions, specifications and conformity criteria,
587 BS EN 450-1:2005 + A1:2007.
- 588 [29] Fernández-Jiménez, A., & Palomo, A. (2003). Characterisation of fly ashes. Potential reactivity as
589 alkaline cements ☆. *Fuel*, 82(18), 2259-2265.
- 590 [30] Kumar, R., Kumar, S., & Mehrotra, S. P. (2007). Towards sustainable solutions for fly ash through
591 mechanical activation. *Resources, Conservation and Recycling*, 52(2), 157-179.
- 592 [31] Escalante-García, J. I., Fuentes, A. F., Gorokhovskiy, A., Fraire-Luna, P. E., & Mendoza-Suarez, G. (2003).
593 Hydration Products and Reactivity of Blast-Furnace Slag Activated by Various Alkalis. *Journal of the*
594 *American Ceramic Society*, 86(12), 2148-2153.
- 595 [32] Richardson, I. G., Brough, A. R., Groves, G. W., & Dobson, C. M. (1994). The characterization of
596 hardened alkali-activated blast-furnace slag pastes and the nature of the calcium silicate hydrate
597 (CSH) phase. *Cement and Concrete Research*, 24(5), 813-829.
- 598 [33] Ismail, I. (2013). Durability as a function of microstructure of alkali-activated slag/fly ash binders, PhD
599 thesis, University of Melbourne.
- 600 [34] Richardson, I. G. (1999). The nature of CSH in hardened cements. *cement and concrete research*,
601 29(8), 1131-1147.
- 602 [35] Provis, J. L. (2014). Geopolymers and other alkali activated materials: why, how, and what? *Materials*
603 *and structures*, 47(1-2), 11-25.
- 604 [36] Yip, C. K., Lukey, G. C., & Van Deventer, J. S. J. (2005). The coexistence of geopolymeric gel and
605 calcium silicate hydrate at the early stage of alkaline activation. *Cement and Concrete Research*, 35(9),
606 1688-1697.

607 [37] Garcia-Lodeiro, I., Palomo, A., Fernández-Jiménez, A., & Macphee, D. E. (2011). Compatibility studies
608 between NASH and CASH gels. Study in the ternary diagram $\text{Na}_2\text{O}-\text{CaO}-\text{Al}_2\text{O}_3-\text{SiO}_2-\text{H}_2\text{O}$. *Cement and*
609 *Concrete Research*, 41(9), 923-931.